Topological enhancement of exciton-polariton coherence with non-Hermitian morphing

Ruiqi Bao,* Huawen Xu, Wouter Verstraelen, and Timothy C. H. Liew[†]
Division of Physics and Applied Physics, School of Physical and Mathematical Sciences,
Nanyang Technological University, Singapore 637371, Singapore

The non-Hermitian skin effect (NHSE) has been intensely investigated over the past few years and has unveiled new topological phases, which have no counterparts in Hermitian systems. Here we consider the hybridization between the NHSE in an exciton-polariton waveguide and a localized defect mode. By tuning the non-Hermiticity, we find that the resulting ground-state of the system is both spatially extended and energetically separated from other modes in the system. When polariton lasing occurs in the system, we find an enhanced spatial coherence compared to regular waveguides, which is robust in the presence of disorder.

Introduction. When cavity photons and quantum well excitons are strongly coupled they morph into hybrid particles known as exciton-polaritons [1, 2], which exhibit properties from both of their constituents. The photonic component supports a light effective mass, resulting in an energy separation of modes (in finite-sized systems), which further supports spatial coherence when polariton condensation populates states in a narrow energy range. The photonic part further allows dissipation in the system, which makes the system non-Hermitian. To exist, polariton condensates must be supported by a gain in the system. This is typically arranged by a non-resonant laser exciting hot electron-hole pairs that relax in energy feeding the excitonic component of polaritons. While initially requiring cryogenic cooling, polariton condensation is now routinely observed at room temperature [3–7].

With advances in etching techniques, it has become common practice to confine polaritons in arbitrary spatial potentials, including waveguides and lattices. The availability of polariton lattices has supported the field of topological polaritons, where the typical objective is to engineer a bandstructure such that it isolates a small number of states in a bandgap using topology to ensure robustness against structural variations and disorder. Su-Schrieffer-Heeger chains [8–10], Chern insulators [11–13], valley Hall effects [14, 15], spin-valley Hall effects [16], antichiral edge states [17, 18], and higher-order topological insulators (corner states) [19–21] have all been studied in exciton-polariton systems. In many of these geometries, the different options for coupling polariton states, including the spatial overlap of lattice sites and spin-orbit coupling play a crucial role.

Being non-Hermitian systems, polaritons also support a variety of non-Hermitian topological effects, including: exceptional points [22–24], bound-state-in-continuum modes [25], non-Hermitian skin effect (NHSE) [26–29], non-Hermitian corner modes [30], and end-mode lasing [31]. In the NHSE, unlike in the Hermitian case, all eigenstates are localized at the boundary of the sys-

tem, which suppresses backscattering in propagation [32–35]. A topological invariant known as the winding number is used to explain the non-trivial topology of NHSE. Furthermore, it has been proposed that combining systems with different topologies allows for morphed states [36, 37]. This shows that non-Hermitian topology not only provides opportunities for engineering complex energy spectra but also offers a platform to spatially control the eigenstates.

Engineering of the complex energy spectra is potentially useful for the design of polariton lasers, which aim to exploit the coherence of light emitted when a polariton condensate forms. Here it is important to realize that while simple theoretical models often consider a polariton condensate as a single energy state, real polariton condensates have a finite bandwidth. Already in the equilibrium case, a phase with perfect spatial coherence is impossible in a uniform trap in less than three dimensions at finite temperature [38]. Additional fluctuations from the driven-dissipative nature of polaritons are generally believed to make the situation worse [39]. This is especially so in materials used for room temperature operation, where fluctuations due to dissipation are stronger and it is necessary to work with short pulses to avoid sample overheating. The highest coherence of polariton lasers requires isolating the lasing mode in energy, which has been achieved in a trapped geometry (and using a sub-wavelength grating to separated different polarized states) [40]. While this technique is good for enhancing temporal coherence [41], the trapping of the condensate necessarily limits spatial coherence to the trap size. In spatially extended systems, it is common for multiple condensates to appear within an energy bandwidth. While spectrally resolving each mode shows a good spatial coherence of each mode [42], an ideal polariton laser would show spatial coherence without such spectral filtering. It is also understood that disorder limits the range of spatial coherence in spatially extended systems [43] (although it could be compensated with active feedback loops [44]). One could hope that the aforementioned topological polariton systems could aid in enhancing spatial coherence by allowing a spatially extended state to exist in a bandgap robust in the presence of dis-

^{*} Corresponding author: ruiqi002@e.ntu.edu.sg

[†] Corresponding author: timothyliew@ntu.edu.sg

order. However, the topological properties of Hermitian systems do not manifest specifically in the ground state (which we take as the desired state for polariton lasing) and the non-Hermitian examples considered so far do not operate with real energy bandgaps.

In this work we consider the hybridization of a polariton waveguide supporting the non-Hermitian skin with the modes of an intentional defect (trap). The aim is to morph the ideal properties of the trap, namely the presence of a ground state well-isolated in energy, with the ideal properties of the skin effect, namely the spreading of its wavefunctions over a controllable localization length. We find theoretically that the system can undergo polariton lasing in the ground state. This allows us to predict an enhanced spatial coherence length compared to that of a regular polariton waveguide. As is expected of most topological systems, we also find robustness of the attained spatial coherence in the presence of disorder.

Model. It was pointed out in [27] that the NHSE can be attained in polariton systems by arranging a phase dependent coupling between two chains of modes with different gain/loss. Examples of realizing such a model include using the coupling between spin states in chains of elliptical micropillars [26], the coupling between vortex modes in chains of polariton rings [28], and most recently the coupling of spin states using Rashba-Dresselhaus spin-orbit coupling (RDSOC) [45, 46] in liquid crystal filled microcavities [47]. The latter proposal has pointed out that the NHSE can occur in continuous waveguides, without a lattice. While our results should not depend on the precise underlying mechanism of the NHSE, the latter proposal will serve best our purpose given that spatial coherence was previously considered in similar onedimensional waveguide [43, 48] geometries and it will avoid modulation of the spatial coherence function by the presence of a lattice. Within such a model, the evolution of polaritons is described by:

$$i\hbar \frac{\partial \Psi_{\pm}}{\partial t} = \left(-\frac{\hbar^2 \nabla^2}{2m} + V \mp 2i\alpha \frac{\partial}{\partial x} - i\gamma_{\pm}\right) \Psi_{\pm} + \Delta_T \Psi_{\mp}, \tag{1}$$

Here Ψ_{\pm} is the wavefunction of polaritons with \pm spin (corresponding to the circular polarization of emitted light). m is the effective mass; V is a two-dimensional spatial potential profile of our considered microcavity, which is deeper inside the waveguide region (-20 meV, grey area as shown in Fig. 1(a)); α is the strength of RDSOC; Δ_T is the X-Y splitting existed in the microcavity; and γ_{\pm} correspond to the decay rates of spin up and down polaritons.

It is instructive to first consider the system in a Hermitian regime, neglecting the loss term ($\gamma_{\pm} = 0$), which gives the dispersion shown in Fig. 1(b). The colorbar used in the figure is calculated according to the degree of circular polarization S_z , which is defined as:

$$S_z = \frac{|\Psi_+|^2 - |\Psi_-|^2}{|\Psi_+|^2 + |\Psi_-|^2}.$$
 (2)

In this situation, time-reversal symmetry is preserved, however, opposite spins propagate in opposite directions. This is a signature behaviour of the topological spin Hall effect, which is further considered in the supplemental material (SM).

Typically in a polariton system, the spin up and spin down decay rates would be the same. However, this changes if we apply a circularly polarized non-resonant pump, which serves as gain. In our calculations, we introduce a spin up polarized, spatially uniform incoherent pump, resulting effectively in $\gamma_+ < \gamma_-$. We calculate the eigenstates' spatial distribution and find that, different from the Hermitian case (Fig. 1(d)), all eigenstates are localized at the right end of the waveguide as shown in Fig. 1(e). Introducing a spin down polarized pump would reverse this localization. This phenomenon known as the NHSE has no counterpart in Hermitian systems. To prove its topological nature, we calculate the complex energy spectrum under both a periodic boundary condition (PBC) and open boundary condition (OBC) as shown in Fig. 1(c). We find that the complex energy spectrum from the PBC forms a closed loop, which is a signature behaviour of the NHSE [49]. In the NHSE, it is expected that all injected polaritons propagate along the same direction (right in this case). The time dynamics of polaritons is further considered in the SM.

Morphing of the defect mode. The interplay between the NHSE and the topological edge state in the SSH lattice has been theoretically proposed [36] and realized in experiments [37]. Here, we consider the interplay between the NHSE and a trivial defect ground state. The defect state is governed by a region with deeper potential than the rest of the waveguide. This could be realized by coupling a micropillar to the waveguide or engineering a region with stronger light-matter coupling [41].

Given that the defect has a deeper potential, the ground state of the system could be expected to be localized in the defect. When $\delta \gamma = 0$ ($\delta \gamma = \gamma_+ - \gamma_-$) as the case without NHSE, the ground state's spatial profile is shown in Fig. 2(b). The spatial profile of this state changes drastically if we increase $\delta \gamma$. When $\delta \gamma$ is not sufficiently large, the mode will be slightly pulled into the waveguide area as shown in Fig. 2(c). Upon further increasing the decay difference, we find the mode extends within the whole waveguide at the right of the defect (Fig. 2(d)). Eventually, with a larger $\delta \gamma$, the mode becomes localized at the right end, similar to other modes within the waveguide (Fig. 2(e)). This effect occurs due to the competition between defect's trapping and localization of the NHSE. The localization length of the NHSE depends on the value of $\delta \gamma$. The skin modes become more localized when $\delta \gamma$ increases. The enhancement of localization at the right end compensates for the decay of the defect mode resulting in the delocalized behaviour. When $\delta \gamma$ is large enough, the NHSE dominates and the ground state becomes localized again.

Lasing in the extended defect mode. The drivendissipative nature of polaritons offers an excellent plat-

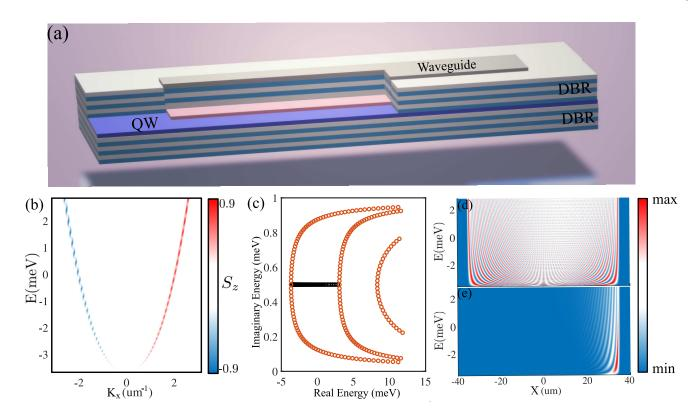


FIG. 1. (a) The schematic figure of a microcavity with an etched waveguide. The microcavity is formed by two sets of Distributed Bragg Reflectors (DBRs) sandwiching a quantum well (QW). (b) Calculated band structure with the consideration of RDSOC, where S_z represents the circular polarization. (c) Complex energy spectra calculated under different boundary conditions: orange points for PBC and black points for OBC. (d) and (e) Eigenstates' spatial distribution in the Hermitian and non-Hermitian cases respectively. Parameters: $m = 2.285 \times 10^{-5}$ of the free electron mass, $\Delta_T = 6$ meV, $\alpha = 1.7$ meV. For (b) and (d), $\gamma_{\pm} = 0$; for (c) and (e), $\gamma_{+} = 1$ meV, $\gamma_{-} = 0$.

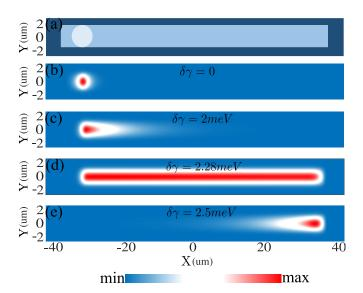


FIG. 2. (a) The schematic figure of a waveguide with a defect on the left-hand side. (b) \sim (e) Spatial distribution of the ground state with different decay rates. Ground state distribution changes drastically from localized inside the defect, dragged into the waveguide, then extended in the waveguide and finally localized at the right end.

form for studying lasing. With the development of topological polaritons, lasing in the topological edge mode, such as the SSH edge mode in a one-dimensional lattice and the chiral edge state in a two-dimensional lattice, has been proposed and realized [50, 51]. In this work, we achieve lasing in the extended defect mode in the presence of the NHSE. By considering the circularly polarized incoherent pump and nonlinear decay, the polariton wavefunction is described by:

$$i\hbar \frac{\partial \Psi_{\pm}}{\partial t} = (1 - i\beta) \left[\left(-\frac{\hbar^2 \nabla^2}{2m} + V \mp 2i\alpha \frac{\partial}{\partial x} \right) \Psi_{\pm} + \Delta_T \Psi_{\mp} \right] + i(P_{\pm} - \gamma) \Psi_{\pm} - i\alpha_1 |\Psi_{\pm}|^2 \Psi_{\pm}.$$
 (3)

Here, β represents energy relaxation [52], iP_{\pm} denotes the circular polarized incoherent pump, and α_1 is the nonlinear decay. The relaxation term causes the extended ground state to have the highest gain, which leads to lasing at the desired extended morphed state. To achieve the NHSE, we select the incoherent circularly polarized pump to be spatially uniform with different strengths $(P_{+}=3.3~meV,P_{-}=0)$, thus creating different effective decay rates. The steady state is shown in Fig. 3(a), where polaritons are distributed al-

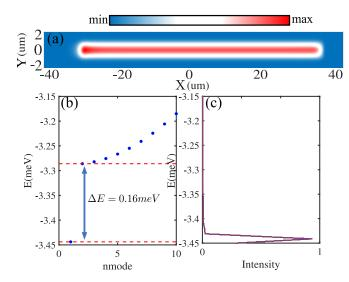


FIG. 3. (a) The steady state's spatial distribution obtained from Eq. (3). The polaritons are uniformly distributed all over the waveguide like the case of Fig. 2(d). (b) Eigenenergies solved in the linear case ($\alpha_1=0$). The energy bandgap between ground state and others is around 0.19 meV. (c) Intensity of polaritons as a function of energy. Parameters: $\beta=0.5, \alpha=1.7$ $meV, \Delta_T=6$ $meV, \alpha_1=1$ $\mu eV \mu m^2, P_+=3.3$ $meV, P_-=0$.

most uniformly throughout the waveguide. Notice that this distribution is similar to the extended state shown in Fig. 2(d). We then calculate the polariton intensity as a function of energy by Fourier transforming the wavefunction Ψ_{\pm} obtained from Eq. (3). Subsequently, we sum up all the intensity along the real space. As shown in Fig. 3(c), the intensity distribution in energy from Fig. 3(a) reveals a peak at around -3.45~meV, which is similar to the extended defect state's eigenenergy calculated by diagonalizing the linear Hamiltonian as shown in Fig. 3(b). This further proves that we have obtained polariton lasing in the extended defect state.

Spatial coherence in an extended defect mode. Owing to the deeper potential, the ground state of the defect carries less energy than the ground state of the waveguide. This energy difference creates a bandgap of around 0.2meV. As a result, after the ground state morphing, it is not only distributed all over the waveguide but is also energetically separated from other modes. This unique property enables the possibility of achieving large-area spatial coherence. We calculate the spatial coherence, $g_1(dx, dy)$ using the formula:

$$g_1(dx, dy) = \frac{\sum_n \Psi_n^*(x, y) \Psi_n(x + dx, y + dy) e^{-\frac{(E_n - E_g)^2}{\delta E^2}}}{\sqrt{I(x, y)I(x + dx, y + dy)}},$$
(4)

$$I(x,y) = \sum_{n} |\Psi_n(x,y)|^2 e^{-\frac{(E_n - E_g)^2}{\delta E^2}}.$$
 (5)

This formula is equivalent to that used in [53], however,

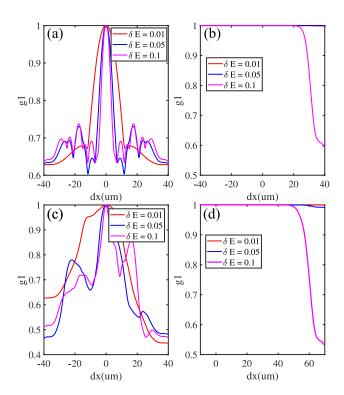


FIG. 4. (a) and (b) Spatial coherence calculated from Eq. (4-5) in a normal cavity case and the NHSE morphing case under different strengths of fluctuations respectively. (c) and (d) Spatial coherence calculated in presence of same strength of disorder in a normal cavity and the NHSE morphing case.

assuming a Gaussian energy distribution function. One might've expected a Bose-Einstein distribution, however, it was shown that this results in a poor fit to experiments given the non-equilibrium nature of polariton systems [53]. Here I(x,y) is the intensity profile of polaritons, E_n is the energy of the modes, E_g is the energy of the ground state, δE is the energy fluctuation. If δE is infinitesimally small corresponding to a perfect condensate, g_1 will equal to 1. In the calculation, we take the reference point (x,y) as the point that has the highest intensity.

In a typical cavity, because of the continuous energy spectrum, more than one mode is excited simultaneously, which results in coherence decay, as shown in Fig. 4(a). It's important to note that with a larger δE , g_1 drops more rapidly. In comparison, the ground state morphing mode displays better coherence all over the waveguide due to the separation of energy and the extended distribution nature. When δE is small, almost just the ground state is excited and g_1 is nearly one in the whole waveguide. Of course if δE is increased too much, coherence will drop, first at the right end of the waveguide. This can be interpreted as other skin modes being excited, which are dominantly localized at the right edge of the waveguide. Note that the coherence remains high throughout the left region of the waveguide.

A well-known advantage of topological systems is the robustness of their states with respect to disorder (provided that the disorder strength is within the topological bandgap). In Fig. 4(c) and (d), we compare the spatial coherence in a regular waveguide and our morphing mode system in the presence of disorder (added as a random potential). We notice that the morphing mode still presents high spatial coherence, which shows the robustness to disorder. In comparison, the breakdown of spatial coherence with the same strength of disorder is also shown in Fig. 4(c) for a regular waveguide.

Conclusion. We consider the hybridization of non-Hermitian skin effect modes and a trapped mode in exciton-polariton waveguides. Because of the competition between the trap and NHSE, the localized defect ground state can become extended inside the waveguide. We then show that lasing can be obtained in the extended defect mode. The large bandgap of this ground state and the large area distribution properties make it possible to achieve a significant spatial coherence length, considerably enhanced compared to non-topological systems, especially in the presence of disorder.

Acknowledgement. The work was supported by the Ministry of Education, Singapore (Grant No. MOE-T2EP50121-0020).

- H. Deng, H. Haug, and Y. Yamamoto, Rev. Mod. Phys. 82, 1489 (2010).
- [2] I. Carusotto and C. Ciuti, Rev. Mod. Phys. 85, 299 (2013).
- [3] H. Deng, G. Weihs, C. Santori, J. Bloch, and Y. Yamamoto, Science 298, 199 (2002).
- [4] S. Christopoulos, G. B. H. von Högersthal, A. J. D. Grundy, P. G. Lagoudakis, A. V. Kavokin, J. J. Baumberg, G. Christmann, R. Butté, E. Feltin, J.-F. Carlin, and N. Grandjean, Phys. Rev. Lett. 98, 126405 (2007).
- [5] S. Kéna-Cohen and S. R. Forrest, Nature Photonics 4, 371 (2010).
- [6] R. Su, C. Diederichs, J. Wang, T. C. H. Liew, J. Zhao, S. Liu, W. Xu, Z. Chen, and Q. Xiong, Nano Letters 17, 3982 (2017).
- [7] R. Su, S. Ghosh, J. Wang, S. Liu, C. Diederichs, T. C. H. Liew, and Q. Xiong, Nature Physics 16, 301 (2020).
- [8] T. H. Harder, M. Sun, O. A. Egorov, I. Vakulchyk, J. Beierlein, P. Gagel, M. Emmerling, C. Schneider, U. Peschel, I. G. Savenko, S. Klembt, and S. Höfling, ACS Photonics 8, 1377 (2021).
- [9] R. Su, S. Ghosh, T. C. H. Liew, and Q. Xiong, Science Advances 7, eabf8049 (2021).
- [10] P. Kokhanchik, D. Solnyshkov, T. Stöferle, B. Piętka, J. Szczytko, and G. Malpuech, Phys. Rev. Lett. 129, 246801 (2022).
- [11] C.-E. Bardyn, T. Karzig, G. Refael, and T. C. H. Liew, Phys. Rev. B 91, 161413 (2015).
- [12] A. V. Nalitov, D. D. Solnyshkov, and G. Malpuech, Phys. Rev. Lett. 114, 116401 (2015).
- [13] S. Klembt, T. H. Harder, O. A. Égorov, K. Winkler, R. Ge, M. A. Bandres, M. Emmerling, L. Worschech, T. C. H. Liew, M. Segev, C. Schneider, and S. Höfling, Nature 562, 552 (2018).
- [14] O. Bleu, D. D. Solnyshkov, and G. Malpuech, Phys. Rev. B 96, 165432 (2017).
- [15] W. Liu, Z. Ji, Y. Wang, G. Modi, M. Hwang, B. Zheng, V. J. Sorger, A. Pan, and R. Agarwal, Science 370, 600 (2020).
- [16] R. Banerjee, S. Mandal, and T. C. H. Liew, Phys. Rev. B 103, L201406 (2021).
- [17] S. Mandal, R. Ge, and T. C. H. Liew. Phys. Rev. B 99, 115423 (2019).
- [18] R. Bao, S. Mandal, H. Xu, X. Xu, R. Banerjee, and T. C. H. Liew, Phys. Rev. B 106, 235310 (2022).

- [19] R. Banerjee, S. Mandal, and T. C. H. Liew, Phys. Rev. Lett. 124, 063901 (2020).
- [20] J. Wu, S. Ghosh, Y. Gan, Y. Shi, S. Mandal, H. Sun, B. Zhang, T. C. H. Liew, R. Su, and Q. Xiong, Science Advances 9, eadg4322 (2023).
- [21] Y. Zhang, Y. V. Kartashov, L. Torner, Y. Li, and A. Ferrando, Opt. Lett. 45, 4710 (2020).
- [22] T. Gao, E. Estrecho, K. Y. Bliokh, T. C. H. Liew, M. D. Fraser, S. Brodbeck, M. Kamp, C. Schneider, S. Höfling, Y. Yamamoto, F. Nori, Y. S. Kivshar, A. G. Truscott, R. G. Dall, and E. A. Ostrovskaya, Nature 526, 554 (2015).
- [23] W. Gao, X. Li, M. Bamba, and J. Kono, Nature Photonics 12, 362 (2018).
- [24] R. Su, E. Estrecho, D. Biegańska, Y. Huang, M. Wurdack, M. Pieczarka, A. G. Truscott, T. C. H. Liew, E. A. Ostrovskaya, and Q. Xiong, Science Advances 7, eabj8905 (2021).
- [25] N. H. M. Dang, S. Zanotti, E. Drouard, C. Chevalier, G. Trippé-Allard, M. Amara, E. Deleporte, V. Ardizzone, D. Sanvitto, L. C. Andreani, C. Seassal, D. Gerace, and H. S. Nguyen, Advanced Optical Materials 10, 2102386 (2022).
- [26] S. Mandal, R. Banerjee, E. A. Ostrovskaya, and T. C. H. Liew, Phys. Rev. Lett. 125, 123902 (2020).
- [27] S. Mandal, R. Banerjee, and T. C. H. Liew, ACS Photonics 9, 527 (2022).
- [28] H. Xu, K. Dini, X. Xu, R. Banerjee, S. Mandal, and T. C. H. Liew, Phys. Rev. B 104, 195301 (2021).
- [29] X. Xu, H. Xu, S. Mandal, R. Banerjee, S. Ghosh, and T. C. H. Liew, Phys. Rev. B 103, 235306 (2021).
- [30] X. Xu, R. Bao, and T. C. H. Liew, Phys. Rev. B 106, L201302 (2022).
- [31] P. Comaron, V. Shahnazaryan, W. Brzezicki, T. Hyart, and M. Matuszewski, Phys. Rev. Res. 2, 022051 (2020).
- [32] S. Yao and Z. Wang, Phys. Rev. Lett. 121, 086803 (2018).
- [33] C. H. Lee and R. Thomale, Phys. Rev. B 99, 201103 (2019).
- [34] Y. Yi and Z. Yang, Phys. Rev. Lett. 125, 186802 (2020).
- [35] L. Li, C. H. Lee, S. Mu, and J. Gong, Nature Communications 11, 5491 (2020).
- [36] W. Zhu, W. X. Teo, L. Li, and J. Gong, Phys. Rev. B 103, 195414 (2021).
- [37] W. Wang, X. Wang, and G. Ma, Nature **608**, 50 (2022).

- [38] P. C. Hohenberg, Phys. Rev. **158**, 383 (1967).
- [39] Q. Fontaine, D. Squizzato, F. Baboux, I. Amelio, A. Lemaître, M. Morassi, I. Sagnes, L. Le Gratiet, A. Harouri, M. Wouters, I. Carusotto, A. Amo, M. Richard, A. Minguzzi, L. Canet, S. Ravets, and J. Bloch, Nature 608, 687 (2022).
- [40] S. Kim, B. Zhang, Z. Wang, J. Fischer, S. Brodbeck, M. Kamp, C. Schneider, S. Höfling, and H. Deng, Phys. Rev. X 6, 011026 (2016).
- [41] M. Wurdack, E. Estrecho, S. Todd, C. Schneider, A. G. Truscott, and E. A. Ostrovskaya, Phys. Rev. Lett. 129, 147402 (2022).
- [42] D. N. Krizhanovskii, K. G. Lagoudakis, M. Wouters, B. Pietka, R. A. Bradley, K. Guda, D. M. Whittaker, M. S. Skolnick, B. Deveaud-Plédran, M. Richard, R. André, and L. S. Dang, Phys. Rev. B 80, 045317 (2009).
- [43] F. Manni, K. G. Lagoudakis, B. Pietka, L. Fontanesi, M. Wouters, V. Savona, R. André, and B. Deveaud-Plédran, Phys. Rev. Lett. 106, 176401 (2011).
- [44] J. D. Töpfer, I. Chatzopoulos, H. Sigurdsson, T. Cookson, Y. G. Rubo, and P. G. Lagoudakis, Optica 8, 106 (2021).
- [45] M. Król, K. Rechcińska, H. Sigurdsson, P. Oliwa, R. Mazur, P. Morawiak, W. Piecek,

- P. Kula, P. G. Lagoudakis, M. Matuszewski, W. Bardyszewski, B. Piętka, and J. Szczytko, Phys. Rev. Lett. **127**, 190401 (2021).
- [46] Y. Li, X. Ma, X. Zhai, M. Gao, H. Dai, S. Schumacher, and T. Gao, Nature Communications 13, 3785 (2022).
- [47] P. Kokhanchik, D. Solnyshkov, and G. Malpuech, arxiv 2303.08483 (2023).
- [48] J. Fischer, I. G. Savenko, M. D. Fraser, S. Holzinger, S. Brodbeck, M. Kamp, I. A. Shelykh, C. Schneider, and S. Höfling, Phys. Rev. Lett. 113, 203902 (2014).
- [49] Z. Gong, Y. Ashida, K. Kawabata, K. Takasan, S. Higashikawa, and M. Ueda, Phys. Rev. X 8, 031079 (2018).
- [50] Y. V. Kartashov and D. V. Skryabin, Phys. Rev. Lett. 122, 083902 (2019).
- [51] P. St-Jean, V. Goblot, E. Galopin, A. Lemaître, T. Ozawa, L. Le Gratiet, I. Sagnes, J. Bloch, and A. Amo, Nature Photonics 11, 651 (2017).
- [52] E. Estrecho, T. Gao, N. Bobrovska, M. D. Fraser, M. Steger, L. Pfeiffer, K. West, T. C. H. Liew, M. Matuszewski, D. W. Snoke, A. G. Truscott, and E. A. Ostrovskaya, Nature Communications 9, 2944 (2018).
- [53] O. Tsyplyatyev and D. M. Whittaker, physica status solidi (b) 249, 1692 (2012).